Journal of Alloys and Compounds 493 (2010) 240–245

Contents lists available at ScienceDirect

Journal of Alloys and Compounds

journal homepage: www.elsevier.com/locate/jallcom

Surfactant-assisted synthesis of $Cd_{1-x}Co_xS$ nanocluster alloys and their structural, optical and magnetic properties

R. Sathyamoorthy[a,*], P. Sudhagar[a], A. Balerna[b], C. Balasubramanian[c], S. Bellucci[b], A.I. Popov[d,e], K. Asokan[f]

[a] R & D Department of Physics, Kongunadu Arts & Science College, Coimbatore, Tamilnadu 641 029, India
[b] INFN-Laboratori Nazionali di Frascati, Via E. Fermi 40000044, Frascati, Italy
[c] Facilitation Centre for Industrial Plasma Technologies, Institute for Plasma Research, Bhat, Gandhinagar 382428, India
[d] Institute of Solid State Physics, University of Latvia, 8 Kengaraga Str, LV-1063 Riga, Latvia
[e] Institite Laue-Langevin BP 1566, ru Jules Horowitz, 38042 Grenoble Cedex 9, France
[f] Inter University Accelerator Centre, Aruna Asaf Ali Marg, New Delhi 110 067, India

ARTICLE INFO

Article history:
Received 22 October 2009
Received in revised form 8 December 2009
Accepted 10 December 2009
Available online 22 December 2009

Keywords:
Nanoclusters
Diluted magnetic semiconductors
Electronic structure
CdS

ABSTRACT

We report the synthesis of Co-doped CdS nanoclusters ($Cd_{1-x}Co_xS$) for different doping concentrations ($x = 0.10$, 0.20 and 0.30) and characterization of their structural, optical, and magnetic properties. The structural properties studied by X-ray diffraction revealed hexagonal-greenockite structure and a decrease of the lattice parameters (a and c) with doping, showing incorporation of Co in the lattice. The morphology of the nanoclusters was studied by scanning electron microscopy. The optical absorption studies, using diffused reflectance spectroscopy, revealed that Co doping modifies the absorption band edge. Ferromagnetic phase was observed in the magnetization measurements at room-temperature due to high carrier concentration. X-ray absorption near edge fine structure measurements at the sulfur (S) K-edge of the Co-doped samples revealed that the valence remains divalent and that there are some changes with Co doping in the spectral intensity.

1. Introduction

Current research in the field of magnetic materials aims to obtain room-temperature ferromagnetic (FM) semiconductors for spintronics devices [1]. This approach exploits the spin of the electron in addition to its charge to enhance the functionalities of microelectronics. Diluted magnetic semiconductors (DMS) in II–IV semiconductor systems are particularly interesting for this purpose, since doping of magnetic ions in these systems is more effective than metal oxide systems. Presence of magnetic ions modifies electron transport phenomena of host II–VI semiconductor systems and thus influences the energy levels of *d* or *f*-like open shells with respect to the Fermi level and band edges. It is well known that position as well as degree of electron localization of the magnetic shells are reflected in the competition between two effects *viz.* (a) on-site Coulomb repulsion between the electrons and (b) delocalizing influence of mixing (hybridization) between extended states and the magnetic orbital [1]. The magnitude of orbital mixing is related to the hybridization between delocalized band electrons in the *p*-valence orbital and the localized *d*-orbital for the paramagnetic ion (Fe, Mn and Co) in a tetrahedral crystal field of II–VI semiconductor systems [2–8]. This could be the result of the magnetic coupling exhibited in these systems. Particularly, in Co^{2+} doped II–VI systems (Cd based) *p–d* hybridization gives rise to stable antiferromagnetic coupling via a superexchange mechanism [9,10].

In this perspective, $Cd_{1-x}Co_xS$ alloys can be considered to be a viable material for the successful realization of spintronic devices. Recently, growth of Co-doped CdS thin films has been demonstrated by ion implantation [11] and spray pyrolysis [12] techniques. While these studies show evidence that cobalt strongly influences the optical and magnetic properties, synthesis of good quality films is hindered by the formation of secondary phases. It is in fact reported in Ref. [12] that oxidation is one of the limiting factors during thin film deposition, which leads to the formation of secondary CoO precipitates. This would have a strong effect on the magnetic behavior of the resultant $Cd_{1-x}Co_xS$ system [12]. Thus use of pre-synthesized $Cd_{1-x}Co_xS$ powders or colloidal nanocrystals as a source material for the growth of $Cd_{1-x}Co_xS$ films is highly desirable. Furthermore, it is believed that facial synthesis of desired $Cd_{1-x}Co_xS$ alloy powder would serve as an efficient source material for obtaining its films without altering DMS properties. Therefore, it is necessary to optimize the facile synthesis conditions to derive the DMS behavior in $Cd_{1-x}Co_xS$ alloys. Besides, in chemical

* Corresponding author. Tel.: +91 422 2642095; fax: +91 422 2644452.
E-mail address: rsathya59@gmail.com (R. Sathyamoorthy).

0925-8388/$ – see front matter © 2009 Elsevier B.V. All rights reserved.
doi:10.1016/j.jallcom.2009.12.063

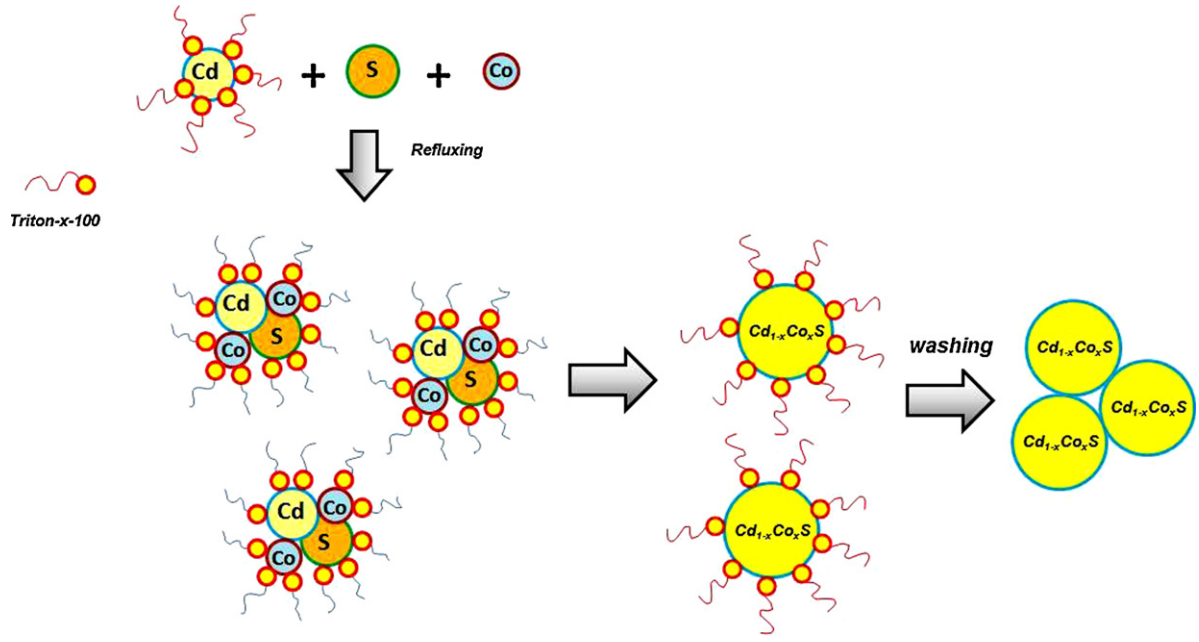

Fig. 1. Schematic growth mechanism of $Cd_{1-x}Co_xS$ at Triton X-100 assisted medium.

synthesis, lattice mismatch between the ionic radii of Co^{2+} (0.74 Å) and Cd^{2+} (0.97 Å) likely to result in isotropic dopant distribution in the system [13]. In order to combat above problem, many researchers preferred different chemical synthesis routes for controlling both the particle size and the doping concentration of Co^{2+} ions in CdS lattice than physical techniques. However, Radivanic and Gamelin [13] have shown that normal soft chemical processing does not render cobalt substitution in a CdS matrix and the dopants are diverted to the surface. Recently this problem was overcome by radiation assisted chemical synthesis [14] technique, though it requires high energy sources.

To circumvent this issue, more attention is needed to find a suitable as well as simple chemical synthesis process that can modify the CdS surface and enhance the doping of Co ions in the CdS lattice resulting in a more efficient DMS alloys. Polyoxyethylene-(10)-tert-octylphenyl ether (Triton X-100) (Fig. 1) is a non-ionic surfactant which is commonly used to synthesize nanostructures of metal nanoparticles, metal chalcogenides, and ceramic oxides [15,16], both as a reducing agent as well as a stabilizer [17,18]. Therefore, in the present work we have made an attempt to utilize Triton X-100 as a surfactant for preparing Co-doped CdS DMS samples. This paper reports the microstructure, electronic structure, optical properties and its interdependence upon magnetic behavior of $Cd_{1-x}Co_xS$ nanoclusters for different Co concentrations synthesized by surfactant-assisted method.

2. Experimental details

Typical synthesis of $Cd_{1-x}Co_xS$ alloys is as follows: a suspension consisting of cadmium dichloride ($CdCl_2$, 50 mM) in 20 ml of Triton X-100 (~24 mM) is prepared. Aqueous solution of thioacetamide in basic medium is added drop by drop to the above suspension under constant stirring at 80 °C in argon atmosphere. The desired amount of aqueous solution of cobalt acetate (0.10 M, 0.2 M and 0.3 M) is injected into the resulting mixture and is refluxed for 12 h and left overnight. By taking in to account the reaction mechanism proposed for the synthesis of CdS nanoparticles by Zhu et al. [19], herein we propose a similar mechanism for the growth of $Cd_{1-x}Co_xS$ nanoclusters as follows:

$$CH_3CSNH_2 + H_2O \rightarrow CH_3(NH_2)C(OH) - SH \quad (1)$$

$$CH_3(NH_2)C(OH) - SH + H_2O \rightarrow CH_3(NH_2)C(OH)_2 + H_2S \quad (2)$$

$$CH_3(NH_2)C(OH)_2 \rightarrow CH_3(NH_2)C = O + H_2O \quad (3)$$

$$H_2S + CdCl_2 \xrightarrow[\text{injection-of-}Co^{2+}\text{-refluxed-at-80}\,^\circ C]{\text{Triton-X-100}} Cd_{1-x}Co_xS + 2HCl \quad (4)$$

Growth mechanism of $Cd_{1-x}Co_xS$ alloys in surfactant-assisted medium is depicted in Fig. 1. Triton X-100 has strong hydrophilic group head and is capped with Cd cation molecules and during the injection of sulfur source, S^{2-} are released slowly, followed by sulfide anions and doping Co ions were binding with Cd^{2+} cations. Thereafter $Cd_{1-x}Co_xS$ alloys will start to form on the surface of the vesicles.

The crystal structure of $Cd_{1-x}Co_xS$ samples was analyzed by X-ray diffractometer (Shimadzu XRD 6000) using CuK_α. Surface morphology of the samples was examined by scanning electron microscopy (JEOL–JSM 6340). Diffused reflectance spectra of $Cd_{1-x}Co_xS$ alloys for different Co doping concentration were recorded using Varian 5000 spectrophotometer. The magnetization measurements were performed in a vibrating sample magnetometer (VSM) (Lakeshore Model 74035) at room temperature. X-ray absorption near-edge structure (XANES) measurements at sulphur *K*-edge on these finely powdered samples were performed at the DRX1 beamline at LNF, Frascati (Italy). The experiment was carried out in transmission mode, at room temperature and in vacuum. During measurements the energy was scanned from 2455 eV to 2490 eV with a step of 0.2 eV. The acquisition time for each energy point was typically set to 1 s and S_8 was used as standard reference for calibration in all these measurements.

3. Results and discussion

3.1. Structural analysis

The X-ray diffraction patterns of pure CdS and $Cd_{1-x}Co_xS$ alloys for different Co doping concentration (x) are presented in Fig. 2(a) and (b), respectively. The observed diffraction peaks in pure CdS sample correspond to hexagonal-greenockite structure (JCPDS 41-1049, $a = 4.140$ Å, $c = 6.719$ Å) and crystal orientations are predominantly along (0 0 2), (1 0 1) and (1 1 0) direction. The absence of individual metal peaks in X-ray diffraction spectra reveals that a single compound or alloy ($Cd_{1-x}Co_xS$) is formed. From Fig. 2(b) it is obvious that the intensity of diffraction peaks was weakened along (1 0 3), (1 1 2) and (2 0 3) directions with increase of Co concentration. It indicates that Co doping has inhibited the crystallization of CdS. From Fig. 2(b), it can be found that the diffraction peak of the (0 0 2) orientation, shifts towards lower angles with the increase of Co content.

The possible reason could be that CdS lattice gets modified and consequently its lattice parameters were altered due to Co doping. The lattice parameters (a and c) of pure CdS and $Cd_{1-x}Co_xS$ samples

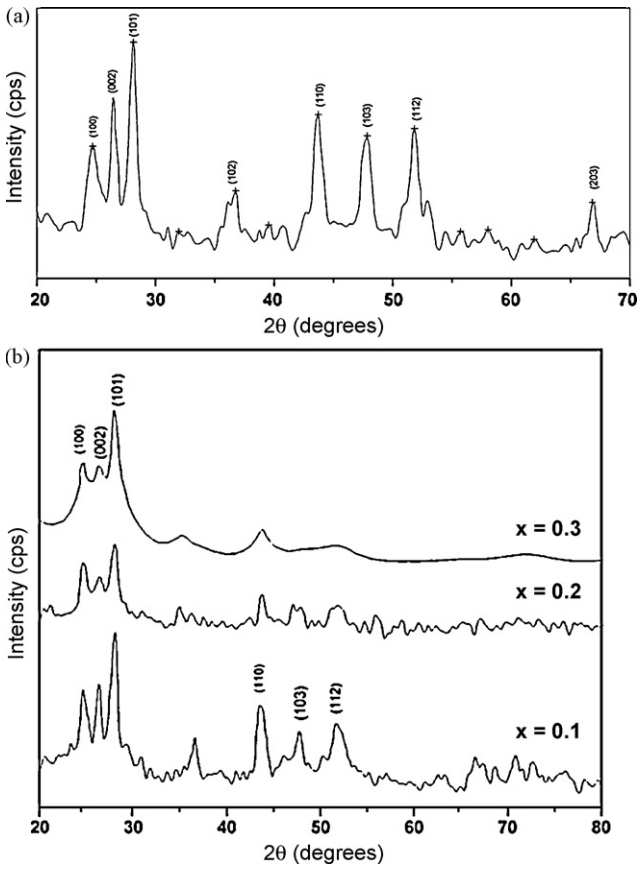

Fig. 2. X-ray diffraction spectra of (a) pure CdS and (b) $Cd_{1-x}Co_xS$ samples.

were estimated using the relation [16]:

$$\sin^2\theta = \frac{\lambda^2}{4a^2}\left[\frac{4}{3}(h^2+hk+k^2)+\frac{l^2}{(c/a)^2}\right] \quad (5)$$

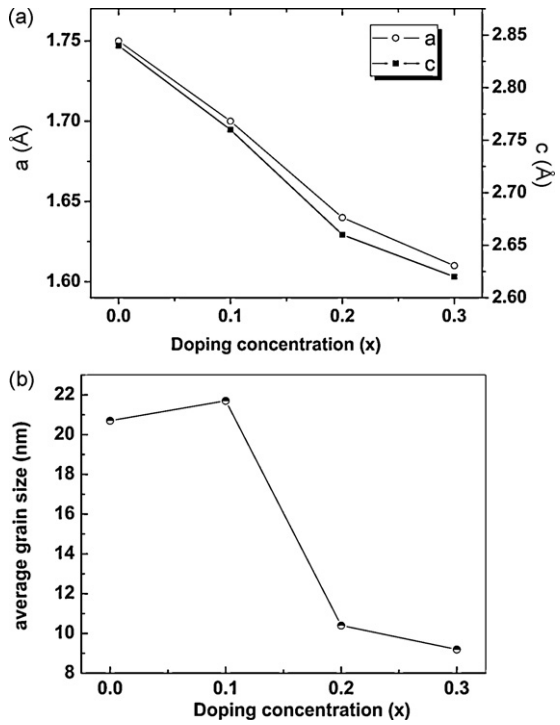

Fig. 3. (a) Lattice parameters and (b) average grain size [estimated using (0 0 2) crystal direction] of pure CdS and $Cd_{1-x}Co_xS$ alloys for different Co doping concentrations (x = 0, 0.1, 0.2 and 0.3).

The estimated lattice parameters a and c are presented in Fig. 3(a). From Fig. 3(a), it is clearly found that the lattice parameters (a and c) decrease with Co concentration. These results imply that the Co^{2+} has been incorporated into the crystal lattice of CdS. As the ionic radius of Co^{2+} (0.74 Å) is smaller than that of Cd^{2+} (0.97 Å) Co^{2+} ions can easily enter into the crystal lattice of CdS and occupy the substitution sites, thus brings contraction in CdS lattice (Fig. 3(a)),

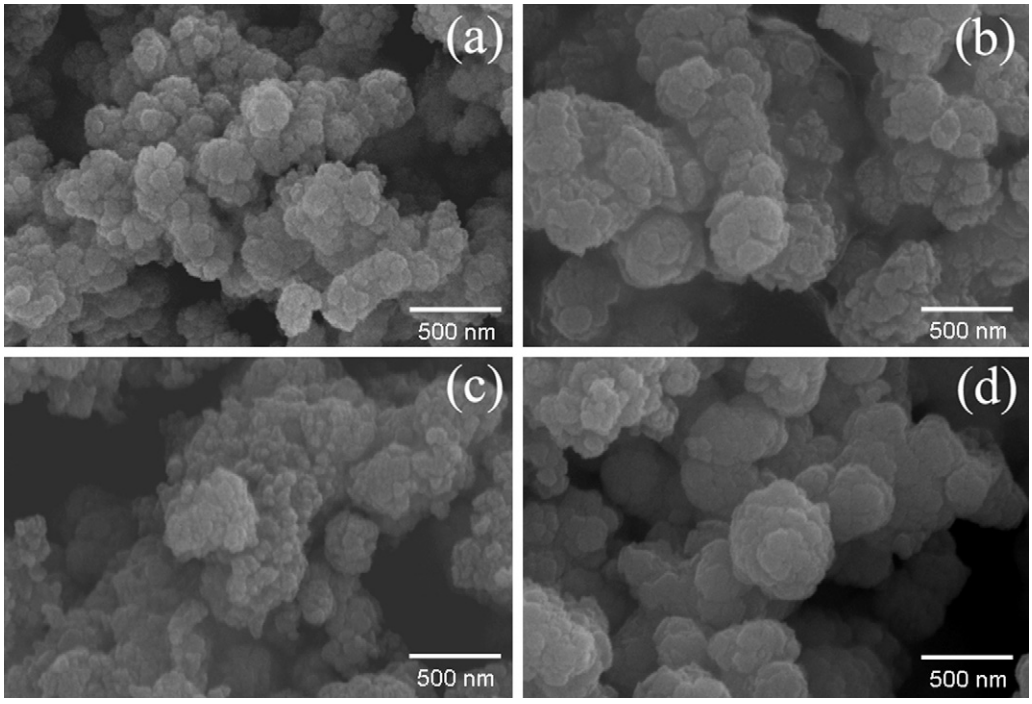

Fig. 4. FE-SEM images of (a) pure CdS, (b) $Cd_{0.9}Co_{0.1}S$, (c) $Cd_{0.8}Co_{0.2}S$, and (d) $Cd_{0.7}Co_{0.3}S$ nanocluster alloys.

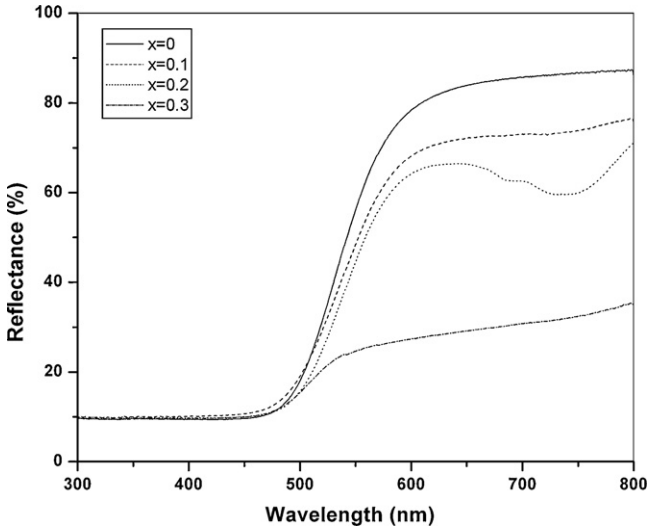

Fig. 5. Diffused reflectance spectra of pure and Co-doped CdS samples.

which is consist with the earlier reports on Co-doped CdS systems [11].

Average grain size of bare CdS and $Cd_{1-x}Co_xS$ samples was estimated using Scherrer formula and is presented in Fig. 3(b). From Fig. 3(b), it is noticed that there is no significant change in the average grain size takes place for low level of Co concentration ($x = 0.1$). Further increase in Co concentration to $x = 0.2$ and $x = 0.3$ leads to a systematic reduction in the grain size from 20 nm to ~10.4 nm and ~9.2 nm, respectively.

3.2. Surface morphology

Fig. 4(a–d) shows the SEM images of pure CdS and $Cd_{1-x}Co_xS$ samples for various Co concentrations. It clearly shows that constituent particles of CdS are agglomerated and leads to the formation of cluster-like patterns (Fig. 4(a)). This may be attributed to removal of Triton X-100 micelles during washing with cyclohexane and ether (Fig. 1), thus leads aggregation of CdS particles and Co ions, thus resulting $Cd_{1-x}Co_xS$ alloys in cluster-like pattern. Recently, there has been considerable interest in metal nanoclusters with sizes of 1–100 nm. In the lower end of the range, clusters tend to assume structures unrelated to macroscopic crystal structures and have novel physical and chemical properties [20]. The literature argue that these metal nanoclusters have reduced melting and sintering temperatures when compared to the bulk materials because of the comparatively high surface-area-to-volume ratio, which allows bonds to readily form between neighboring particles [21]. We believe that the obtained cluster-like $Cd_{1-x}Co_xS$ alloys in the present work may exhibit unique properties in diluted magnetic device applications.

3.3. Optical properties

Diffused reflectance spectra of $Cd_{1-x}Co_xS$ nanoclusters for different Co doping concentration ($x = 0$, 0.1, 0.2 and 0.3) were recorded using spectrophotometer and the resulting spectra are shown in Fig. 5. A blue shift in the absorption onset of about 0.26 eV compared to the bulk CdS [2.4 eV] can be noticed in undoped CdS nanoclusters. This result is a direct consequence of the quantum confinement effect associated with the small particle size. The absorption onset of $Cd_{0.90}Co_{0.10}S$ could turn to red shift with increase in x values. The value of band gap energy for different Co concentrations in $Cd_{1-x}Co_xS$ nanoclusters obtained from the diffused reflectance spectra at room temperature are given in Table 1.

Table 1
Band gap energy and magnetic parameters of $Cd_{1-x}Co_xS$ samples ($x = 0.1$, 0.2 and 0.3).

Co doping concentration (x)	Band gap energy (eV)	M_s (emu/g)	$H\Theta$ (O_e) (Gauss)
0	2.56	–	–
0.1	2.65	0.053	254.85
0.2	2.57	0.025	7815.5
0.3	2.70	0.676	86

The observed band gap bowing effect may due to exchange interactions of the conduction and valence band electrons with the Co^{2+} d electrons. Presence of localized magnetic ions in semiconductor alloys leads to exchange interaction between s–p band electrons and the Co^{2+} d electrons. It plays a dual role in determining optical properties. (i) The band gap of the compound is altered depending upon the concentration of cobalt ions and (ii) the 3d levels of transition metal ions are located in the band gap region, and d–d transition dominates the spectrum [22].

3.4. Magnetic properties

The magnetization measurements were performed at room temperature and the observed magnetic signal of different Co-doped CdS nanoclusters are presented in Fig. 6(a)–(c) and the magnetic parameters of $Cd_{1-x}Co_xS$ such as saturation of magnetization (M_s) and coercivity ($H\Theta$) for different doping concentration were estimated from the hysteresis curve and are presented in Table 1. In the dilute limit ($x < 0.01$), the dopant spins can be treated as isolated domains, resulting in paramagnetic behavior for the DMS system. As the dopant concentration increases, the onset of dopant–dopant spin interactions, arising primarily from nearest neighbor coupling (J_{NN}) via a superexchange mechanism, causes a deviations from the classical paramagnetic spin glass antiferromagnetic regime [23]. At higher concentrations, cobalt-doped DMS systems have been observed to exhibit a type III antiferromagnetic lattice, arising from strong spin coupling due to strong exchange between Co^{2+} and S atoms in the hexagonal lattice [23]. Therefore, values of J_{NN} (Co^{2+}–Co^{2+}) correlate with the Co^{2+}doping concentrations (x), which suggest an enhanced super exchange interaction with increasing Co^{2+} concentration. This phenomenon is responsible for exhibiting high magnetization ($M_s = 0.676$ emu/g) in $Cd_{0.7}Co_{0.3}S$ sample. Thus, in the present work Co-doped CdS samples with $x = 0.3$ could result in better ferromagnetic behavior than the lower doping concentrations ($x = 0.1$ and 0.2).

3.5. X-ray absorption near-edge structure studies

X-ray absorption near-edge structure (XANES) spectroscopy provides "fingerprint" information about oxidation state, the nature of the empty molecular orbitals of the absorbing atom. The number of empty molecular orbitals and their energy positions are characteristic for different chemical species. XANES is therefore a technique for identifying different molecular species [24]. Sulfur K-edge XANES provides a unique approach for determining the chemical forms of sulfur in materials and their local bonding with neighboring cations. This spectrum is dominated by dipole-allowed ($\Delta l = \pm 1$) bound-state transitions of the 1s electron (for a K-edge) to vacant molecular orbitals of substantial p orbital character. Hence, the near-edge spectrum provides a sensitive probe of electronic structure and thus of the chemical form. Sulfur shows particularly rich near-edge spectra, due to valence p-orbitals. The relatively sharp line-widths at these energies and the large chemical shift (of some 14 eV) span over its range of oxidation states (−2 to +6) [25].

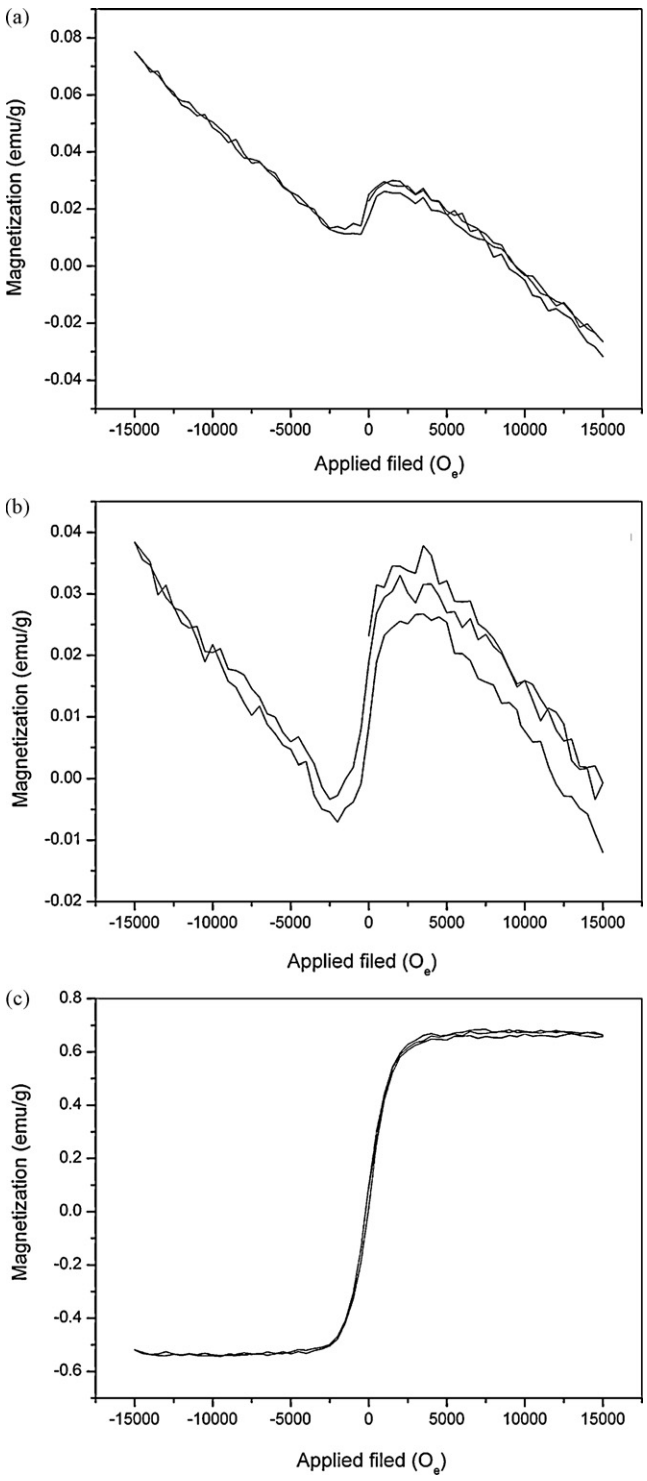

Fig. 6. Ferromagnetic behavior of a nanocluster alloys for (a) $Cd_{0.9}Co_{0.1}S$, (b) $Cd_{0.8}Co_{0.2}S$, and (c) $Cd_{0.7}Co_{0.3}S$.

Fig. 7 shows the normalized XANES spectra at S K-edge of Co-doped CdS nanoclusters. These provide information about the change in the oxidation state of S in these compounds and also change in the bonding of S 3*p* states with Cd/Co 3d states. The major spectral features are marked as 'A' and 'B' and these features are similar in CdS and also Co-doped CdS. However the spectral feature marked 'A' is broad and represents three fine structures which are associated with S-3*p* states hybridized with Cd/Co 3*d* states. As is evident S is divalent and Co enters the lattice as divalent at Cd

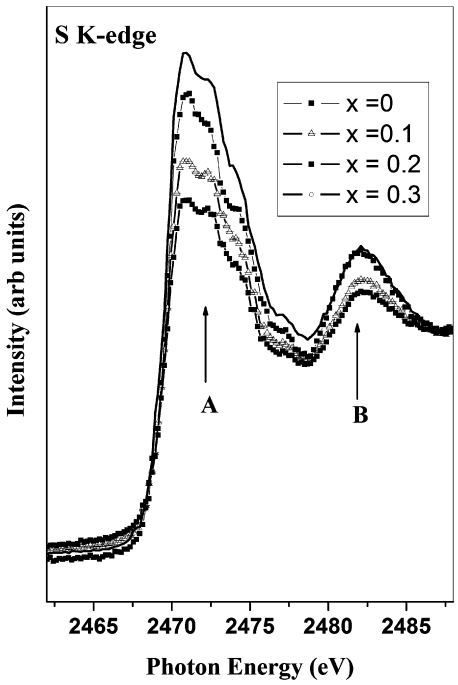

Fig. 7. XANES spectra of pure CdS and $Cd_{1-x}Co_xS$ alloys for different Co doping concentrations ($x = 0, 0.1, 0.2$ and 0.3) [note that the oxidation state of S remains divalent with Co doping and this also indicates that the valency of Co is divalent].

sites which is also a divalent cation. Comparison of intensity of CdS and Co-doped CdS show that density of unoccupied states of S 3*p* states are significantly high in 30% Co-doped CdS nanocrystals and gets reduced considerably for 10 and 20% Co-doped CdS. This also supports that there is change in the hole concentration due to Co doping. Present study is similar to the doping of Mn and Co in ZnS investigated by Pong et al. [26]. The electronic structures can be derived from the Co 3d and S 3p bands of Cd(Co)S alloys from their respective atomic levels. The magnetic–transition metal, Co ion is divalent in Cd(Co)S and exhibits T_d group symmetry and hence Co, 3d states are split into e doublets and t_2 triplets by the crystal field. Based on symmetry consideration, the 3p electrons of neighboring S atoms do not have p–d hybridization with the Co 3d(e) states. This explains why there is no variation in the spectral features of S K-edge except in their intensity.

4. Conclusions

In conclusion, Co^{2+} ions were doped with CdS nanoclusters by surfactant-assisted synthesis technique. The lattice parameters of CdS nanoclusters were altered with respect to Co doping concentrations and it exhibits hexagonal-greenockite structure. Grain size of the CdS nanoclusters increases with increase in Co doping concentration. *sp–d* spin exchange interaction has been observed in $Cd_{1-x}Co_xS$ samples and this result in the band gap bowing effect in DMS alloys. The structural, optical, and magnetic properties of $Cd_{1-x}Co_xS$ nanoclusters demonstrate DMS behavior.

Acknowledgments

This work was supported under Transnational Access to Research Infrastructures program (TARI project No. 43), Laboratori Nazionali di Frascati (LNF), INFN, Frascati, Italy.

References

[1] Lewicki, A.I. Schindler, J.K. Furdyna, T.M. Giebultowicz, in: M. Jain (Ed.), Diluted Magnetic Semiconductors, World Scientific Publishing Co. Pvt. Ltd., Singapore, 1991, pp. 410–460.
[2] K. Liu, J.Y. Zhang, X. Wu, B. Li, B. Li, Y. Lu, X. Fan, D. Shen, Physica B 389 (2007) 248–251.
[3] D. Sreekantha Reddy, K. Narasimha Rao, K.R. Gunasekhar, Y. Dwarakanadha Reddy, P. Sreedhara Reddy, J. Alloys Compd. 461 (2008) 34–38.
[4] A.V. Kouzema, M. Froba, L. Chen, P.J. Klar, W. Heimbrodt, Adv. Funct. Mater. 15 (2004) 168–172.
[5] Mycielski, L. Kowalczyk, R.R. Gałązka, Roman Sobolewski, D. Wang, A. Burger, M. Sowinska, M. Groza, P. Siffert, A. Szadkowski, B. Witkowska, W. Kaliszek, J. Alloys Compd. 423 (2006) 163–168.
[6] Lewicki, A.I. Schindler, P.M. Shand, B.C. Crooker, J.K. Furdyna, Phys. Rev. B 44 (1991) 6137–6140.
[7] U. Alvera, E. Bacakszb, E. Yanmaz, J. Alloys Compd. 456 (2008) 6–9.
[8] V. Ladizhansky, V. Lyahovitskaya, S. Vega, Phys. Rev. B 60 (1999) 8097–8104.
[9] Y. Dwarakanadha Reddy, D. Sreekantha Reddy, B.K. Reddy, R.V.S.S.N. Ravikumar, D.R. Reddy, J. Alloys Compd. 470 (2009) 12–15.
[10] K.M. Hanif, R.W. Meulenberg, G.F. Strouse, J. Am. Chem. Soc. 124 (2002) 11495–11502.
[11] S. Chandramohan, A. Kanjilal, S.N. Sarangi, S. Majumder, R. Sathyamoorthy, T. Som, J. Appl. Phys. 106 (2009) 063506–063511.
[12] E. Bacaksiz, M. Tomakin, M. Altunbas, M. Parlak, T. Colakogluc, Physica B 403 (2008) 3740–3745.
[13] P.V. Radovanovic, D.R. Gamelin, J. Am. Chem. Soc. 123 (2001) 12207–12214.
[14] K.A. Bogle, S. Ghosh, S.D. Dhole, V.N. Bhoraskar, L. Fu, M. Chi, N.D. Browning, D. Kundaliya, G.P. Das, S.B. Ogale, Chem. Mater. 20 (2008) 440–446.
[15] K. Zhu, L. Huang, J. Zhu, Z. Zhuang, Spectrochim. Acta A 69 (2008) 566–571.
[16] Y. Ding, X. Liu, R. Guo, Mater. Res. Bull. 43 (2008) 748–758.
[17] A. Pal, Talanta 46 (1998) 583–587.
[18] T.K. Sau, A. Pal, T. Pal, J. Phys. Chem. B 105 (2001) 9266–9272.
[19] J. Zhu, M. Zhou, J. Xu, X. Liao, Mater. Lett. 47 (2001) 25–29.
[20] F.F. Shi, Michal Bulkowski, K.C. Hsieh, Nanotechnology 18 (2007) 265301–265306.
[21] S.B. Fuller, E.J. Wilhelm, J.M. Jacobson, J. Microelectromech. Syst. 11 (2002) 54–60.
[22] L. Levy, J.F. Hochepied, M.P. Pileni, J. Phys. Chem. 100 (1996) 18322–18326.
[23] J.K. Furdyna, J. Appl. Phys. 64 (1988) R29–R64.
[24] J.C. Fuggle, J.E. Inglesfield, Unoccupied Electronic States, 69 ed., Springer Verlag, Berlin, 1992.
[25] www.usask.ca/geology/nfaculty/ip/sulfur-examples.pdf.
[26] W.F. Pong, R.A. Mayanovic, J.K. Kao, H.H. Hsieh, J.Y. Pieh, Y.K. Chang, K.C. Kuo, P.K. Tseng, J.F. Lee, J. Phys. IV 7 (1997), pp. C2–1147.